communications earth & environment

Article

A Nature Portfolio journal

https://doi.org/10.1038/s43247-026-03401-6

Seismic events drive pollution in Japan Trench hadal basins

Sara Trotta[1,2], Jan Schwarzbauer[3], Alessandro M. Michetti[1,4] & Piero Bellanova[2]

Hadal trenches, the deepest regions of the ocean, have long been considered remote sinks for organic matter and pollutants. However, recent evidence suggests these environments are more dynamic, influenced by both natural events and human activity. Here we present a geochemical assessment of organic and inorganic pollutants in surface sediments from seven basins along the Japan Trench axis, at depths greater than 7000 metres below sea level. We show that earthquake-triggered sediment flows are a major mechanism delivering anthropogenic pollutants, including polycyclic aromatic hydrocarbons, dichlorodiphenyltrichloroethane metabolites, hopanes, and trace metals, into the trench. While slow background transport contributes to deep-sea contaminant accumulation, episodic, high-energy sediment-gravity flows appear to dominate pollutant delivery in this ultra-deep environment. These findings reveal that pollution in hadal trenches is not simply passive accumulation but can be driven by seismic events, linking human activity on land to biogeochemical processes in tectonically active marine settings.

Hadal trenches, oceanic regions exceeding 6000 ms below sea level (mbsl) in depth, represent the most extreme and least explored environments on Earth[1]. Defined by intense hydrostatic pressure, low temperatures, and limited oxygen availability, these deep-sea depressions host unique geological and ecological dynamics[2–4]. Traditionally viewed as isolated sediment-starved bathymetric features with minimal exchange with surrounding ocean basins, recent evidence indicate active connectivity and material flux between hadal zones and the coast[5]. Due to their steep, narrow, V-shaped morphology, hadal trenches function as terminal depocenters[6,7], where sediments and organic matter (OM) originating from upper ocean layers and continental sources gradually accumulate over time[8,9]. In addition to accumulating natural sediment and OM, hadal environments in the vicinity of densely populated and industrialised regions, such as the Japanese archipelago, serve as long-term sinks for anthropogenic pollutants[10–12]. Many of these compounds are hydrophobic and readily adsorb onto particulate matter, including sinking marine snow and sedimentary detritus[13]. In recent years, however, it has become increasingly evident that deep-sea pollutant accumulation is shaped by multiple interacting sediment-transport processes. Beyond slow background settling, high-energy sediment-gravity flows such as turbidity currents have been shown to transport substantial quantities of particulate pollution, including microplastics and associated contaminants, to great ocean depths[14–16]. At the same time, persistent bottom currents, contourite systems, and even human-modified sediment pathways can influence the redistribution and burial of contaminants, underscoring that deep-sea trenches function as dynamic rather than passive repositories of anthropogenic material[17]. In the Japan Trench (JT), earthquake-induced turbidites, resulting from surficial remobilisation in shallower areas[18,19], mass movements forming mass transport deposit (MTDs) and sediment-gravity flows[20], represent particularly noteworthy pathways[9], delivering large pulses of sediment, organic carbon and associated contaminants to hadal environments[5,11,12,20]. These rapid, high-energy depositional events dominate sedimentary input over decadal to centennial timescales. Other contributing processes include long-range advection via deep ocean currents and boundary layer flows[21,22], though these typically operate at slower rates and over broader spatial and temporal scales. In addition, studies from the neighbouring Miura-Boso forearc basin document the influence of persistent bottom currents and contourite deposition on deep-marine sedimentation, suggesting that steady along-slope and along-trench flows may further redistribute and partially rework event-derived deposits over longer timescales[23]. Notably, bottom currents or contourites have not been described yet for the Japan Trench. Modern environmental pollutants in the marine system are broadly categorised into three primary categories: (i) inorganic contaminants (e.g. heavy metals)[24], (ii) persistent organic pollutants POPs[12,25] (e.g. polycyclic aromatic hydrocarbons (PAHs), pesticides), and (iii) anthropogenic litter, notably plastic waste[26]. Despite the growing interest in deep-sea research, comprehensive assessments on pollutant transport, accumulation, and long-term environmental effects in hadal trenches remain limited. Current knowledge is

[1]Department of Science and High Technology (DiSAT), University of Insubria, Como, Italy. [2]Institute of Neotectonics and Natural Hazards, RWTH Aachen University, Aachen, Germany. [3]Institute of Organic Biochemistry in Geo-Systems, RWTH Aachen University, Aachen, Germany. [4]INGV Istituto Nazionale di Geofisica e Vulcanologia, Sezione di Napoli, Napoli, Italy. e-mail: p.bellanova@nug.rwth-aachen.de

constrained by the technological and logistical challenges of operating in these environments, as well as by high associated costs. Only sporadic studies have documented contamination in trench sediments or bioaccumulation in hadal biota[27], leaving substantial knowledge gaps regarding the fate and behaviour of pollutants in the deepest parts of the ocean. Moreover, most existing studies focus on the deepest points of well-known trenches, overlooking the spatial heterogeneity within individual trench basins. Recent findings suggest that local hydrodynamics (e.g., bottom currents) and variations in trench morphology significantly influence the deposition and distribution of pollution-bearing particles along the trench axis[28]. This implies that data from trench maxima may not be representative of the system as a whole, emphasising the need for spatially resolved investigations.

In this study, we present a detailed assessment of organic and inorganic pollutants inventories in hadal superficial sediment (1.0 cm to 52.0 cm depth below ocean floor), collected from seven basins along the JT axis (water depth >7.4 km) (Fig. 1 and Supplementary Fig. 2) during International Ocean Discovery Program (IODP) Expedition 386. The JT is known as a depositional basin for high-density mass transport deposits triggered by recent tsunamigenic megathrust seismic events ($M_W > 9$)[9,29]. We focus on the detection and distribution of anthropogenic pollutants as well as diagnostic marker compounds, including polycyclic aromatic hydrocarbons (PAHs), hopanes, DDT metabolites, and hazardous trace metals (e.g. Cr, Ni, Cu, As, Cd, Te, Pb). By analysing contaminant profiles and transport mechanisms, we aim to advance the current understanding of deep-sea pollution pathways and provide insights into the anthropogenic fingerprint on one of the planet's most remote and extreme environments.

Results and discussion

Pollutant inventory along the Japan Trench

A wide range of anthropogenic contaminants was identified in surficial sediments across the Japan Trench. To characterise human impacts on these hadal habitats, we distinguish between persistent organic pollutants (POPs) and inorganic potentially toxic elements (PTEs). Organic pollutants are further grouped into three categories: (i) petrogenic contaminants, (ii) pesticides, and (iii) technical additives. In a separate subsection, we then describe the distribution of (iv) inorganic PTEs.

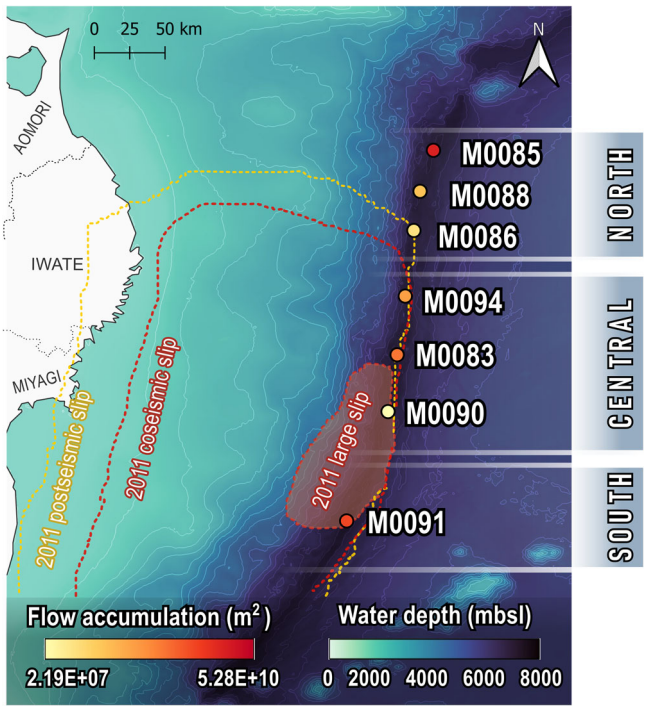

Fig. 1 | Japan Trench sampling overview. IODP Expedition 386 sites along the JT, divided into northern, central, and southern sectors based on past seismic segmentation. Sampling locations are shown relative to water depth (bathymetric data from GEBCO) and modelled flow accumulation (adapted from Kioka et al.[9]). The schematic illustrates the 2011 Tōhoku-Oki earthquake large-slip region (orange polygon), and the coseismic (red dotted line) and postseismic (yellow dotted line) slip areas after Uchida and Bürgmann[70].

Petrogenic contaminants. Among the anthropogenic pollutants detected, petrogenic compounds are identified in sediments from the Japan Trench through source-specific molecular markers, notably polycyclic aromatic hydrocarbons (PAHs) and hopanes. Hopanes are dominated by C_{29}, C_{30}, and C_{31} homologues, with a general decline in abundance from C_{32} to C_{35} (Fig. 2a and Supplementary Fig. 3a). This pattern reflects selective degradation processes and differences in hydrocarbon sources. While this molecular weight trend is common in many sites, it is not consistent across the entire study area. Notably, sites with higher total hopane concentrations do not always display the complete homologue series. For example, despite exhibiting the highest total hopane load, site M0094 shows a pronounced abundance of high molecular weight hopanes (C_{32}-C_{35}), with a relatively lower contribution from lighter homologues. The highest hopane concentrations are observed progressively from south to north along the trench. In addition, surface sediment layers (post-earthquake) generally exhibit the highest levels of hopanes and concentrations diminish with increasing sediment depth. These observations are indicative of increased petrogenic emissions of the recent pollution history and reflect ongoing diagenetic processes and reduced preservation potential with depth. To gain insight into pollution sources, the diagnostic ratio based on *18α(H)-trisnorhopane* (Ts) to *17α(H)-trisnorhopane* (Tm) concentrations (Ts/(Ts+Tm)) was utilised. While this ratio is traditionally used as a thermal maturity indicator for organic facies[30], in this context it aids in identifying mature allochthonous petroleum contamination[31]. Values range from 0.09 to 0.41 (Supplementary Fig. 3b) with notable high ratios exhibited in post-earthquake sediments at sites M0090 and M0091. In contrast, the post-event layer at M0094 presents an intriguing exception, displaying the lowest Ts/(Ts+Tm) ratio across all sites. This result may be attributed to the presence of high concentrations of fresh, immature hydrocarbons, which typically yield lower Ts/(Ts+Tm) ratios[30]. The most likely scenario at M0094 is the coexistence of older, buried hydrocarbons, reflected in more mature signals observed in both pre- and post-event layers, and major recent inputs in the surface sediments[32].

PAHs originating mainly from incomplete combustion processes or fossil fuel contamination tend to bind preferentially to particulate organic matter in coastal and shallow marine sediments. These compounds are introduced through various pathways, including oil spills, urban runoff, and atmospheric deposition[33,34]. In the JT, PAHs have been ubiquitously detected, exhibiting notable spatial variability (Fig. 2b). Site M0094 displays the highest PAH concentrations, followed by M0085 and M0083, suggesting that these basins act as accumulation zones. The elevated contamination at M0094 is likely related to its proximity to the coastline with a narrow shelf, facilitating accelerated pollutant deposition to deeper parts of the ocean. In contrast, more distal sites (e.g. M0086 and M0088) and those with adjacent to the wider Sendai Shelf (e.g. M0090 and M0091), are characterised by lower levels of PAH contamination. In detail, high molecular weight (HMW) PAHs (comprising 4–6 aromatic rings) dominate over low molecular weight (LMW) PAHs (2–3 rings) (Supplementary Table 3), reflecting their stronger affinity for organic-rich substrates and enhanced accumulation. In contrast, LMW PAHs are present at lower concentrations due to their higher solubility in water and preferential partitioning into the dissolved phase. Compositional analysis reveals a complex mixture of both petrogenic and pyrogenic PAHs[35]. The detection of compounds such as *fluoranthene*, *pyrene*, and *retene* suggests more petrogenic contributions, sourced from oil spills or fuel combustion. Meanwhile, elevated levels of *benzo[b]fluoranthene*, *indeno[1,2,3-cd]pyrene*, and *benzo[k]fluoranthene*

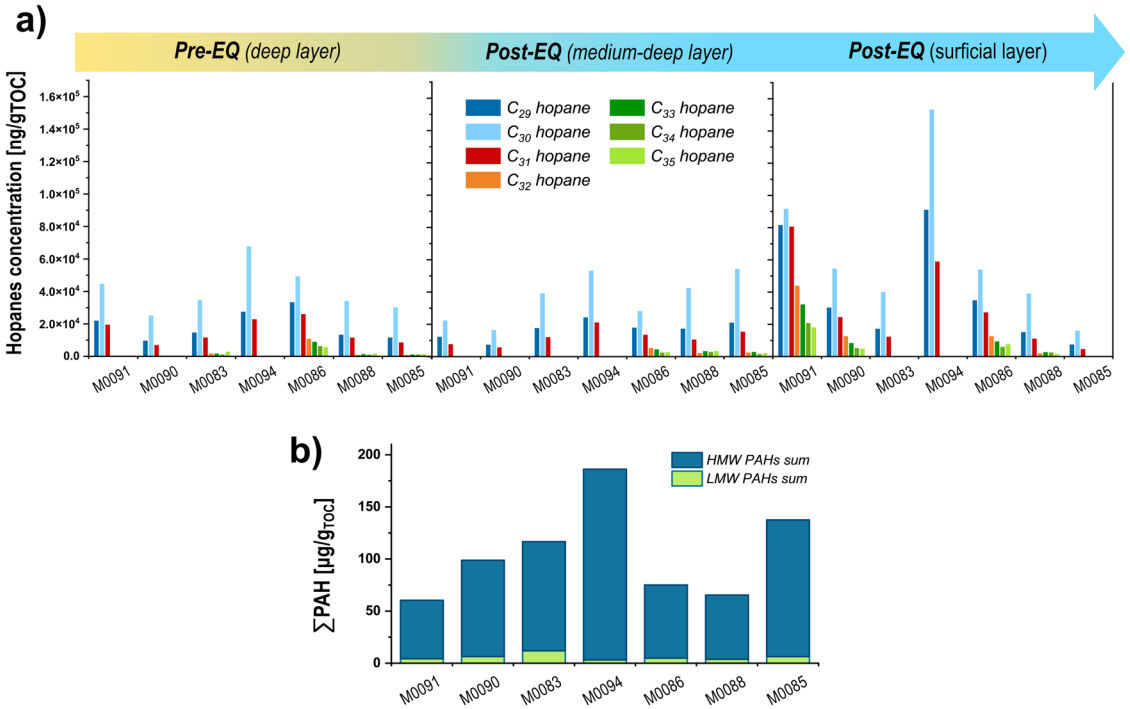

Fig. 2 | Petrogenic pollutants concentrations in sediments along the Japan Trench. a Hopanes fingerprint and concentrations (ng g_{TOC}^{-1}) across sediment layers, categorised into pre-earthquake (Pre-EQ; left panel) and post-earthquake layers (Post-EQ, centre and right panels). Individual hopane compounds are represented by coloured bars corresponding to the legend. **b** Total concentration of polycyclic aromatic hydrocarbons (PAH), showing the sum of identified PAH compounds in each sediment core. Bars are stacked to distinguish PAH classes (heavy molecular weight PAH "HMW", in blue colour, and low molecular weight PAH "LMW", in light green colour).

point to pyrogenic sources, including industrial emissions or volcanic activity. Unlike the more consistent vertical trends observed for hopanes, PAH concentrations do not decrease uniformly with depth.

Pesticides. To date, studies reporting *1,1,1-trichloro-2,2'bis(p-chlorophenyl)ethane* (DDT) and its metabolites (DDX) have largely focused on coastal[36] or shelf-region sediments at substantially shallower water depths[31,37]. A single previous investigation addressed bioaccumulation of these contaminants in endemic amphipods within the Mariana, Mussau, and New Britain trenches[25], but no data exist for the JT. DDT was widely applied as an insecticide from the 1940s until its ban in the 1970s due to its persistence and toxicological impacts[38]. Under aerobic conditions, DDT predominantly degrades into DDE, while anaerobic environments favour DDD formation[39,40]. Consistently, our analysis detected no parent DDT but only its metabolites, *p,p'-dichlorodiphenyldichloroethylene* (*p,p'*-DDE) and *p,p'-dichlorodiphenyldichloroethane* (*p,p'*-DDD). Measured concentrations of *p,p'*-DDE and *p,p'*-DDD varied significantly among sites and sediment depths (Fig. 3), indicating heterogeneous degradation processes. Total DDX concentrations ranged from 24.45 to 1325.32 ng g_{TOC}^{-1}, with *p,p'*-DDE generally dominating, consistent with its environmental persistence[41] (Supplementary Table 3). Site-specific analysis revealed relatively homogeneous concentrations of DDT metabolites in shallow sediment layers. Notable exceptions are sites M0083 and M0091, representing the most and least contaminated sites, respectively. Sites M0083, M0085, and M0094 exhibited notably high proportions of *p,p'*-DDE (80–100% of total DDX, see Supplementary Table 3), suggesting recent deposition from water-column transport or localised microaerobic conditions favouring oxidative degradation. Conversely, elevated *p,p'*-DDD concentrations were predominant in medium-depth layers (post-earthquake sediment), particularly at site M0094, reaching up to 289 ng g_{TOC}^{-1}, suggesting primarily anaerobic degradation conditions or historical contamination.

Technical pollutants. The technical additive, triphenyl phosphate (TPhP) was detected, notably in samples already identified as heavily contaminated by other pollutants. Elevated TPhP concentrations were observed at sites M0094 and M0091, peaking at 7.23 µg g_{TOC}^{-1} (Supplementary Table 3). TPhP is commonly used as a flame retardant and plasticizer, entering the ocean environment through its inclusion in engine and hydraulic oils, as well as impurities in certain oligomeric organophosphorus flame retardants used in plastics and fibres. Considering these diverse sources, it is plausible that TPhP contamination at the trench originate from both terrestrial industrial activities and maritime sources, including vessel exhaust emissions and oil spill[42]. Thus, proximity to the Japanese coastline and high sedimentation rates at these sites likely contribute significantly to contaminant deposition.

Potentially toxic elements. To achieve a comprehensive assessment of pollution in the JT environment, we analysed potentially toxic elements (PTEs)[43], specifically As, Ag, Cd, Cr, Pb, Te, and Zn, using weakly-bound extraction methods targeting fractions associated with anthropogenic activities[44]. This labile fraction represents the most bioavailable and ecologically relevant portion of these elements, essential for evaluating their potential impacts on deep-sea ecosystems. Unlike total metal content, this fraction directly indicates recent inputs and mobility within the sediment column[45], providing critical insight into the distribution of contaminants along the trench. Spatial and depth-dependent variations in PTEs concentrations were observed, with Zn consistently showing the highest concentrations across all analysed elements. Zn ranged from 66.212 mg kg^{-1} up to 190.449 mg kg^{-1} at core M0094, substantially contributing to the total measured PTE load (224.12 mg kg^{-1}), the highest recorded in this study. Elevated Cr concentrations were also identified, particularly in shallow sediment layers at sites M0086 and M0083, reaching maximum values of 25.693 mg kg^{-1} and 25.645 mg kg^{-1}, respectively, and gradually decreasing with sediment

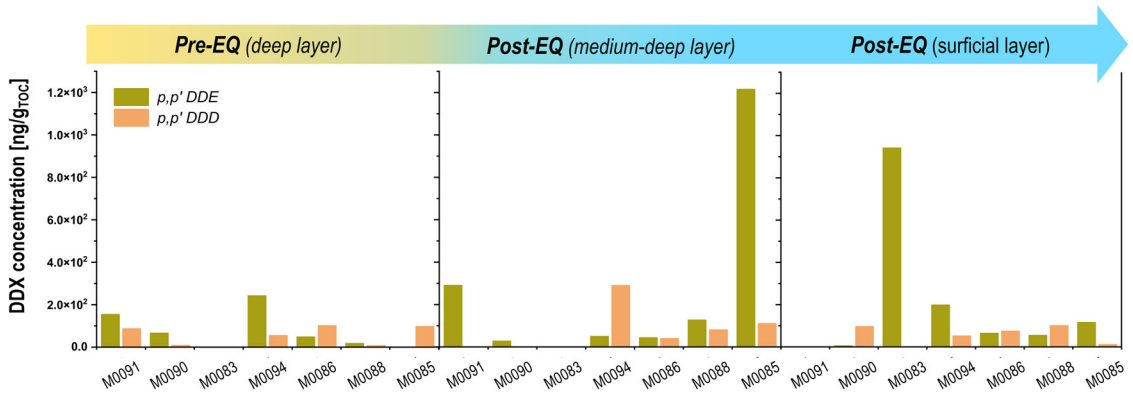

Fig. 3 | Distribution of DDT transformation products (p,p′-DDE and p,p′-DDD). Patterns reveal the presence of legacy pesticide residues at varying depths and sites (p,p'-DDE and p,p'-DDD are respectively represented in green and orange colours).

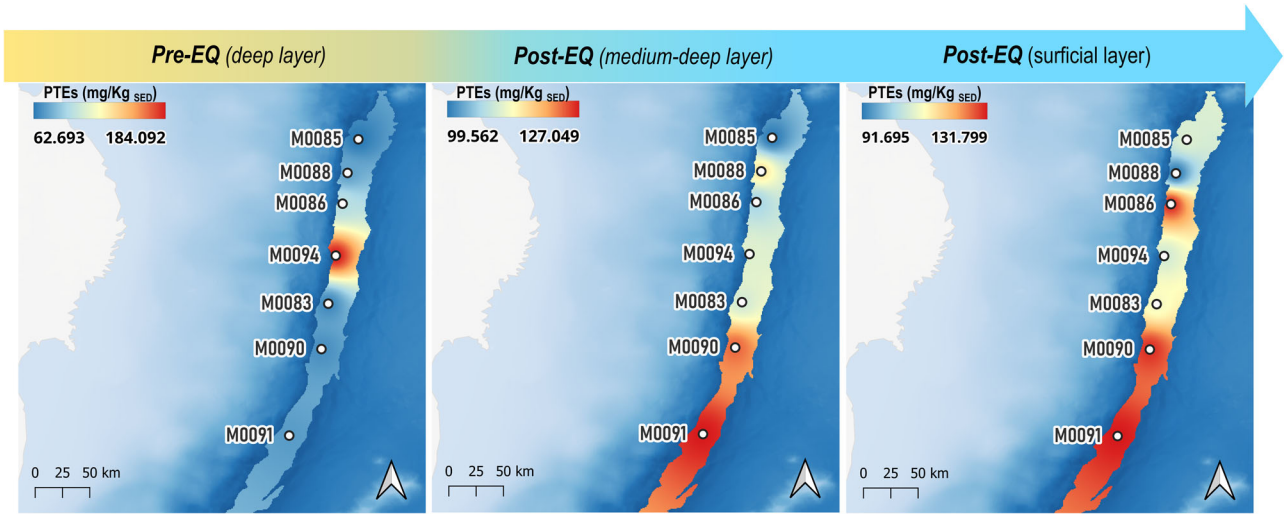

Fig. 4 | Interpolated heatmaps of ΣPTEs concentration patterns. Results for pre-earthquake (Pre-EQ, left panel), and post-earthquake (Post-EQ, centre and right panels) sediment layers. Warmer colours indicate higher concentrations. Sampling sites from IODP Expedition 386 are marked for reference. The gradient arrow indicates the transition from deeper to shallower sediment intervals, highlighting temporal shifts in depositional patterns or contaminant loading across trench segments.

depth. Pb concentrations were generally lower compared to Zn and Cr, showing relatively uniform distributions along the trench but typically higher values in shallow sediment layers, indicative of recent anthropogenic inputs likely derived from coastal or atmospheric sources. However, site M0091 notably deviated from this trend, exhibiting the highest Pb concentration (17.933 mg kg^{-1}) in its shallow layer. This anomaly likely results from the unique conditions of site M0091, being isolated, deep, and associated with high sediment flow accumulation, factors that enhance the deposition and retention of particle-bound contaminants such as Pb. Arsenic concentrations varied between 0.392 and 1.134 mg kg^{-1}, with maxima observed in deeper layers (e.g. M0091), consistent with geochemical remobilisation under reducing conditions. Cd and Ag were present at lower concentrations but followed similar trends, showing localised peaks in deeper sediment layers (Cd: 0.048 mg kg^{-1} at M0085; Ag: 0.233 mg kg^{-1} at M0086), likely reflecting their associations with organic matter and sulphide phases. Te, an inorganic contaminant of emerging environmental concern due to industrial applications, was detected consistently at modest levels across sites (0.005–0.011 mg kg^{-1}). Total PTEs concentrations (Supplementary Table 3), representing the sum of analysed elements per sample (Fig. 4), displayed clear site- and depth-dependent variations, with elevated levels predominantly in shallow and medium-depth sediments, suggesting active accumulation and post-depositional mobility. Comparative analyses highlight Zn, Cr, and Pb as primary contributors to the PTE inventory, whereas As and Cd show notable depth sensitivity. Despite lower absolute concentrations, the persistent detection of Te merits attention due to its growing industrial use and environmental persistence.

Pathways of organic matter and contaminants into the Japan Trench

To better understand the distribution patterns of pollutants across the JT axis and with sediment depth, relationships between contaminants, total organic carbon (TOC) content and sediment flow accumulation were examined. The spatial distribution of TOC across JT basins reflects complex interactions among sediment transport mechanisms and oceanographic processes. Notably, TOC concentrations in the studied sediments are above the global average for deep-sea sediments[46] (typically <0.5%), potentially indicating either elevated high organic matter accumulation in this region[9]. The highest TOC values occur at M0090 (1.8%) and M0086 (1.7%), while the lowest loads are observed at M0091 (0.7%) and M0094 (0.6%) (Fig. 5 and Supplementary Table 3). Although a recent study has demonstrated that oceanic currents through the JT transport dissolved organic carbon (DOC) northward[5], our results do not reflect the expected corresponding increase in particulate TOC towards northern basins. This discrepancy indicates that TOC distribution is likely dominated by sediment-associated transport and

resuspension processes, overriding the influence of steady-state oceanic circulation[28]. In this context, sites with the highest flow accumulation (Fig. 1), such as M0085 (5.28×10^{10} m^2) and M0091 (2.20×10^{10} m^2), exhibit contrasting TOC concentrations. This suggests that sediment influx can result in either enrichment or dilution of TOC, depending on the nature and composition of the sedimentary material deposited. For instance, sites proximal to a mountainous coastline with increased fluvial output onto the short shelf (e.g. M0083 and M0094) see increased influence by organic carbon-rich terrigenous material. However, high-flow accumulation zones (Fig. 1; M0091 and M0085) may have received substantial input from low-organic, coarse-grained sediments, resulting in TOC dilution. This is particularly evident at M0091, where, despite high flow accumulation, TOC remains low, suggesting the dominance of inorganic sediment input or increased storage and degradation of organic material on the wider Sendai Shelf.

Basin morphology further influences TOC preservation. Larger basins (M0085, 25.70 km^2; M0088, 23.30 km^2) prolong organic matter exposure to oxidation due to slower sediment burial and extended organic matter residence times, leading to moderate TOC concentrations (~1.1–1.4%). Conversely, smaller basin areas, such as M0090 (1.80 km^2), experience stronger bottom currents and sediment remobilisation yet still exhibit maximum TOC values, linked to efficient organic carbon deposition. An inverse relationship between TOC and water depth observed at certain sites (e.g. higher TOC at 7445 mbsl – M0090, vs. lower TOC at 7349 mbsl – M0094, Figs. 1 and 5) suggests depth-dependent variability in organic matter preservation. This pattern aligns with recent findings from the JT, that bioturbation processes in hadal zones significantly influence organic matter remineralisation and substrate consistency, potentially driving observed variations in TOC preservation through episodic sediment deposition and benthic colonisation successions[47]. However, inconsistencies across other sites indicate additional local factors and processes also influence this relationship.

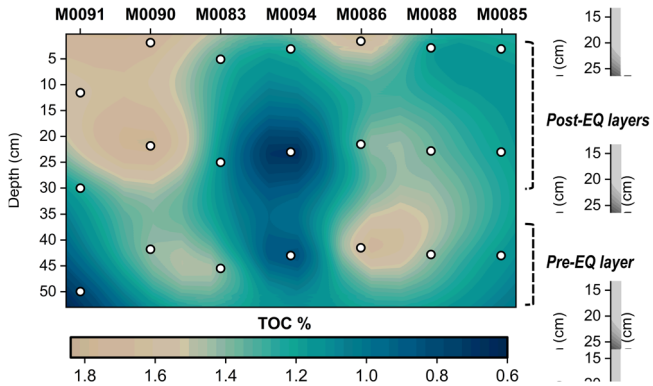

Fig. 5 | Vertical distribution of total organic carbon across sediment depth profiles. The contour plot shows TOC concentrations (TOC %, colour scale) as a function of sediment depth (cm) for each core. Warmer tones represent lower TOC values, while cooler tones indicate higher organic carbon content. White dots denote measured TOC content.

The analysis of biomarkers, specifically marine biomarkers (MB) and corresponding pattern derived from marine-sourced organic matter (e.g. dominance of short-chain *n*-alkanes, $C_{13\text{-}15\text{-}17}$, pristane and phytane) and land biomarkers (LB)[48,49] from terrestrial sources (e.g. long-chain *n*-alkanes, $C_{27\text{-}29\text{-}31}$) reinforce these interpretations, highlighting complex relationships between terrestrial inputs, sediment transport mechanisms, and post-depositional degradation processes. The positive correlation between LB concentrations and TOC at sites such as M0091 and M0090 post-earthquake sediment layers, and both M0086 pre- and post-event sediments, indicates a substantial organic-rich terrigenous contribution (Supplementary Fig. 4b). In contrast, the relatively high concentrations of LB at sites M0094, M0088, and M0085, despite their low TOC values, indicate considerable delivery of terrestrial mineral-rich sediment. The decoupling of TOC and LB concentrations in these basins illustrates the important influence of sediment degradation and oceanographic processes, as well as dilution due to the coarse-grained nature of deposited sediments, emphasising the necessity of integrated multi-proxy approaches for understanding organic carbon dynamics in hadal trenches.

To elucidate the mechanisms governing the transport, accumulation, and fate of pollutants in the JT, we integrated the comprehensive geochemical dataset with site-specific environmental variables (Supplementary Fig. 5). Results reveal coherent relationships among pollutants concentrations, TOC, sediment-flow accumulation, and basin morphology. These associations potentially indicate that pollutant dynamics within the hadal basins are closely linked to event-dominated sedimentary processes documented along the trench[19], including mass-transport deposits (MTDs), turbidity currents, and tsunami-related remobilisation (Fig. 6). These inferences are strongly supported by previous studies that have applied a range of dating techniques to establish clear stratigraphic links between recent event beds and historical megathrust earthquakes, most notably the

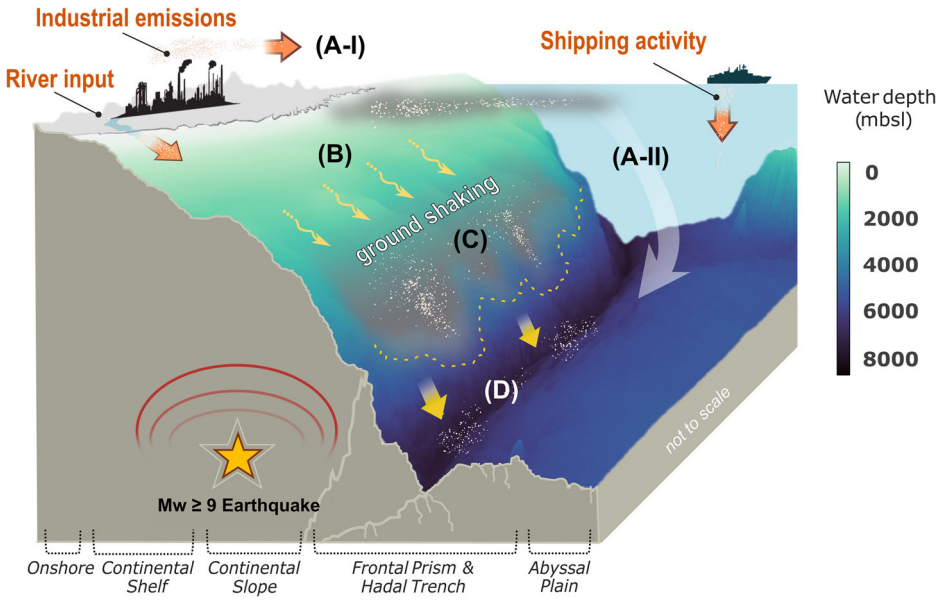

Fig. 6 | Conceptual model of seismic-induced sedimentary and pollution transport processes into the deep-sea. A-I Coastal and onshore located anthropogenic pollution sources with initial transport onto the shelf or during seismic events additional release through destruction and transport via surface water suspension cloud of the tsunami-backwash (**A-II**) Sediment and particle-associated pollution settling out of suspension through the water column. **B** Seismic surficial sediment remobilisation on the shelf and turbidity downslope flow (**C**) Seismically induced submarine mass transports forming mass transport deposits (MTDs) in the deep-sea. **D** Final sink of sediment deposition and associated pollution in the hadal basins of the Japan Trench.

2011 Tōhoku-Oki earthquake[9]. In particular, deposits attributed to the 2011 event, including those associated with the tsunami and aftershock sequence, have been precisely constrained using short-lived radionuclides[50–52]. These studies demonstrate that sediment remobilisation was initiated by prolonged, low-frequency ground shaking, which displaced only the uppermost, organic-rich centimetres of the seafloor across a wide region matching the rupture area[19,50,52–54]. This robust process-based framework provides a chronological and mechanistic foundation for interpreting the geochemical signatures observed in our samples, specifically, the delivery of pollutant-bearing sediments into the trench via earthquake-triggered, surficial remobilisation of anthropogenically enriched shelf material.

In this broader context, recent studies have highlighted that deep-sea pollutant transport can be governed by a combination of mechanisms, including gravity flows[15,16] and contour currents[17]. Our results therefore complement, rather than contradict, emerging evidence that high-energy sediment-gravity flows represent major conduits for particulate pollutants to reach the deep ocean, while recognising that persistent bottom currents may further redistribute fine material after deposition[23]. In this framework, we interpret earthquake-triggered mass-transport and tsunami-backwash processes as the primary pathways (Fig. 6) that deliver pollutant-bearing material from the shelf and upper slope into the hadal basins[50,52], while recognising that steady along-trench bottom currents[23] likely act as a secondary, longer-term agent that redistributes and partially reworks these deposits rather than generating the initial pollutant flux. This interpretation is consistent with work showing that turbidity currents and earthquake-induced slope failures can efficiently transfer organic matter and to abyssal and hadal settings[7,21,52]. Specifically, the strong relation of organic contaminants (e.g. PAHs, hopanes, and DDT metabolites) with TOC and terrestrial biomarkers suggest that pollutant transport occurs predominantly through particle-bound flues originating from continental and coastal sources. Sites showing elevated TOC, extensive hopane homologues, and high DDX concentrations correspond to basins characterised by large sediment-flow accumulation, implying substantial inputs during periods of enhanced sediment remobilisation. The 2011 Tōhoku-Oki earthquake ($M_W > 9$) and previous tsunamigenic seismic events (e.g. 1896 Sanriku-Oki) triggered large-scale sediment displacement[9,29], redistributing organic-rich material from coastal zones via the tsunami backwash[47] and the shelf via surficial remobilisation[52,55] to the trench. Notably, central trench basins, such as M0090 and M0091, exhibit elevated TOC levels, extensive hopane homologue distribution, and high DDT metabolite concentrations, reflecting substantial inputs of allochthonous, petroleum-derived material originating from densely populated and industrialised coastal zones. Moreover, the enrichment in thermally mature hopanes, corroborated by elevated Ts/(Ts+Tm) ratios observed in shallow sediments, strongly supports recent deposition of petrogenic hydrocarbons bypassing traditional diagenetic maturation pathways.

The differentiation among PAH molecular-weight classes further points to multiple transport modes. High-molecular-weight PAHs, being more particle-reactive, are preferentially retained within geomorphological depressions that act as traps during energetic depositional episodes. Their distribution patterns are therefore consistent with downslope transport associated with turbidity flows or tsunami-induced resuspension[9]. In these contexts, basin geometry significantly modulates the long-term PAH retention, independently of local TOC content. Post-depositional degradation of TOC, juxtaposed with the greater resistance of HMW PAHs to degradation, further contributes to observed decoupling between these parameters. Conversely, LMW PAHs display a stronger affinity to TOC, indicative of their enhanced solubility, greater mobility in dissolved phases, and susceptibility to degradation prior to burial. The relatively smooth spatial distribution of TOC, and its weak correlation with known indicators of episodic sediment transport (e.g. high-mass contaminants or sediment flow accumulation), suggests that TOC is less influenced by discrete depositional events but more by continuous biogenic input. Sediments characterised by elevated TOC, such as post-earthquake sediments at M0091 and M0090 and pre-event sediments at M0083, displayed very low or below detection limit (< LOD) concentrations of DDT metabolites. The distribution patterns of DDT metabolites offer additional insights into the post-depositional transformation processes. Elevated concentrations of *p,p'*-DDE observed in TOC-rich sediments (e.g. M0091) imply oxidative degradation pathways under suboxic conditions, whereas increased *p,p'*-DDD levels recorded at pre-earthquake sediment layers or more distal sites (e.g. M0094) indicate reductive transformation occurring under anoxic environments. Importantly, locations such as M0085, characterised by low TOC yet high sediment flow accumulation, contain substantial DDX concentrations, underscoring the critical role of rapid physical sediment transport mechanisms, such as seismically-induced mass transports, superimposing the influence of organic carbon content alone. Such decoupling highlights potential variations in the composition, reactivity, and degradation kinetics of transported material mobilised during seismic-induced or tsunami backwash sediment transport events. Similarly, spatial distributions of PTEs (e.g. Zn, Pb, Cd, Ag, Te, Cr, and As) reveal distinct geochemical signatures reflecting both depositional dynamics and diagenetic processes. PCA results identify a pronounced clustering of Zn, Cd, and Pb with terrestrial and marine biomarkers, suggesting their co-transport with organic-rich particles derived from coastal and fluvial sources during tsunami backwash and submarine seismic mass transport events. Elevated Zn concentrations coinciding with high sediment flow accumulation at sites M0091 and M0094 further reinforce their association with particulate fluxes during rapid energetic depositional episodes. In contrast, elements such as Cr and Ag exhibit prominent depth-dependent enrichment, indicative of post-depositional remobilisation under reducing conditions, facilitating their migration within sedimentary strata following release from organic complexes or sulphide phases. Tellurium consistently correlates with basin morphology and seismic-associated sediment accumulation patterns rather than organic content, pointing toward its persistence and limited mobility under prevailing geochemical conditions in the extreme hadal environment. We also acknowledge that the unique geomorphic and tectonic context of the Japan margin, marked by widespread surficial failures along steep slopes, in combination with highly industrialised coastline and history of pollution, favours the remobilisation of surface sediments enriched in anthropogenic pollutants. This may contrast with other tectonic (e.g., segments of the Chilean, Kaikōura or other subduction margins) or non-seismic settings (e.g. passive margin systems), where thicker landslides or flood-driven flows may mobilise deeper, pre-industrial material with lower anthropogenic signatures.

Collectively, these findings reveal that the transport, deposition, and fate of organic pollutants and PTEs in the JT are governed by a multi-faceted interplay among pollutant-specific physicochemical attributes, seismically-induced sedimentary transport mechanisms (tsunami backwash and submarine mass transport) (Fig. 6), basin morphology and depositional environments, as well as post-depositional biogeochemical transformations under extreme environmental conditions in the hadal deep-sea. The trench functions simultaneously as a selective filter and long-term repository for anthropogenic substances, favouring the burial and preservation of hydrophobic, particle-reactive compounds, while allowing the degradation or remobilisation of more labile species. The observed decoupling between pollutant concentrations and TOC emphasises that, although organic matter plays a significantly role for initial pollutant transport into shallow marine environments, before earthquake-related transport processes, basin morphology and geochemical interactions substantially modulate transport into the trench, and subsequent long-term pollutant retention and cycling within hadal sediments. The physical shaking up and remobilisation of polluted shallow marine shelf sediments (Fig. 6B) in combination with the backwash transport (Fig. 6(A-I)) of freshly released pollution through vast destruction in the coastal area render megathrust earthquakes and the overarching seismic cycle of subduction zones such as the JT impactful for the pollution dispersal and transport into the highly sensitive deep-sea environment and carbon cycle.

Methods

Study area and sample collection

The Pacific Plate is subducting beneath the Okhotsk Plate along the JT at a rate of approximately 8.0–8.6 cm yr^{-1}[56]. The trench trends predominantly north-south to NNE-SSW, extending from its southern origin at the triple junction between the Pacific, Philippine Sea, and Okhotsk Plates, to its northern intersection with the Kuril Trench[57]. The plate interface exhibits erosional characteristics, with subduction erosion driving tectonic subsidence and forming a gently sloping (1°–2° gradient) upper slope terrace that hosts isolated sedimentary basins[58]. The lower slope is steeper, averaging a gradient of ~5°, and is marked by a narrow midslope terrace situated at water depths between 4000 and 6000 m below sea level (mbsl), shaped significantly by active faulting along the subduction margin[59]. The trench floor displays north-south to NNW-SSE-oriented horst-and-graben structures formed due to flexural bending of the subducting Pacific Plate. This structural arrangement produces elongated, physically isolated trench-fill and graben-fill basins characterised by vertical relief on the order of several hundred metres[60].

Giant Piston Corers (GPC), capable of retrieving 40 m-long sediment cores, and mudline Pilot Cores were collected from seven basins along the JT between April and June 2021 during the Offshore phase of IODP Expedition 386 onboard of *R/V Kaimei MSP*[61] (Fig. 1, Supplementary Fig. 1 and Supplementary Table 1). Upon retrieval, core barrels were brought to the surface, sectioned, and subsequently transferred to onboard laboratories for initial processing, non-invasive measurements, splitting and storage[61]. Surficial mudline sediment samples intended for this study were collected during the Personal Sampling Party in November to December 2022 onboard *D/V Chikyu*. Sample material was stored in darkness and frozen at temperatures below −20 °C to prevent microbial alteration and photodegradation until compound extraction.

Geochemical procedures

Organic compounds extraction: pollutants and biomarkers. From each sediment samples, aliquots of wet material (15–20 g) underwent ultrasonic-assisted sequential extraction[62] using 30 mL of ultra-pure (i) acetone, (ii) acetone/*n*-hexane (1:1 vv), (iii) and *n*-hexane. Each extraction step was followed by centrifugation at 1500 rpm for 10 min to facilitate solvent separation. After collecting and combining the extracts in a separation funnel, the aqueous phase was separated by a surplus of *n*-hexane. The organic extract volume was then reduced by rotary evaporation (400 mbar) to a final volume of approximately 1.5–2 mL. The concentrated extracts were dried over a glass microcolumn filled with pre-cleaned, anhydrous, granulated sodium sulphate (Na_2SO_4) and further concentrated to approximately 1 mL. Sulphur was removed by addition of HCl-activated copper powder in ultrasonic agitation (15 min). Both Na_2SO_4 and copper powder were thoroughly cleaned with high-purity acetone and *n*-hexane prior to use. After 16 h, the extracts underwent fractionation using glass microcolumn chromatography packed with 2 g of silica gel powder (J.T. Baker®, silica gel 40 µm) and overnight conditioned at 200 °C. The extracted volume was fractionated into six fractions (B1-B6) eluted via progressive polarity mixtures solutions of *n*-pentane, dichloromethane (DCM) and methanol (MeOH) (Supplementary Table 2). The acidic compounds in fraction 6 were methylated by the addition of 0.5 mL of a methanolic diazomethane solution. Prior to analysis, 50 µL of an internal standard solution, containing 6.0 ng μL^{-1} d_{36}-hexadecane, 5.1 ng μL^{-1} d_{10}-anthracene, and 4.7 ng μL^{-1} d_{12}-chrysene in *n*-hexane, was added to each fraction. The volume was subsequently reduced to 20 µL via evaporation at room temperature.

PTEs extraction. Sediment samples were subjected to ultrasonic-assisted leaching extraction[63]. For each sample, 0.5 g of homogenised sediment was accurately weighed and transferred into 50 mL of 2.5% nitric acid (0.39 M HNO_3). Extractions were carried out in low-density polyethylene (LDPE) tubes placed in an ultrasonic bath and sonicated for 1 h at room temperature (25 °C). Following sonication, the tubes were centrifuged, and the supernatant was carefully sampled. The resulting solution was filtered through a 0.22 µm membrane filter, spiked with rhodium (Rh; Merck, Darmstadt, Germany) as internal standard to compensate eventual instrumental drifts, and subsequently analysed by Inductively Coupled Plasma Mass Spectrometry (ICP-MS). The elements extracted included arsenic (As), silver (Ag), cadmium (Cd), tellurium (Te), chromium (Cr), zinc (Zn), and lead (Pb).

Instrumental analysis

Total Organic Carbon (TOC). The content of total organic carbon (TOC) in each sediment sample was determined using a LiquiTOC II analyzer (Elementar Analysesysteme GmbH, Germany) operated in single analytical run mode. For each analysis, approximately 100 mg of dried and homogenised sediment was accurately weighed into a quartz combustion boat. TOC was quantified by combustion at 550 °C. Instrument calibration was performed prior to each measurement to ensure analytical accuracy.

Organic compounds identification and quantification. The analysis of organic compounds (organic pollutants and specific biomarkers) in all sample fractions was performed using gas chromatography-mass spectrometry (GC/MS). Measurements were conducted on a triple quadrupole GC-MS system (Thermo Scientific™ TSQ™ 8000 Evo) equipped with a ZB-5 fused silica capillary column (30 m × 0.25 mm i.d. x 0.25 µm film thickness; Zebron, Chrompack). For each fraction, 1 µL of extract was injected in splitless mode, and helium was used as gas carries at a constant flow rate of 1.0 mL min^{-1}. The following temperature program was set for GC oven: from a starting temperature of 60 °C with a splitless time of 60 s, temperature was hold for 3 min and then raised following a temperature ramp of 3 °C min^{-1} to 310 °C and again hold for 20 min. Injection, MS transfer-line, ion source, and quadrupole temperature were set at 270 °C, 270 °C, 250 °C, and 150 °C, respectively.

The mass spectrometer operated in full-scan mode (1.5 scans s^{-1}) over a mass range of 35–700 amu, using a positive electron impact ionisation (EI^+) with 70 eV. Individual organic compounds were identified from the non-target screening approach comparing EI^+ mass spectra with reference libraries (NIST/EPA/NIH Mass Spectral Library NIST98; Wiley/NBS Registry of Mass Spectral Data, 4th Ed., electronic versions) and published literature[18,64,65]. Compound identification was further verified by comparison with reference standards, considering gas chromatographic retention times, elution patterns, and retention indices. Quantitation of selected compounds were performed by integration of specific ion chromatograms and applying an external calibration using authentic reference material. Indicive ratios (e.g. of PAHs, CPI) were calculated based on the peak areas.

Surrogate standard compounds were used to correct for retention time drift and inaccuracies in extract and injection volume. The limit of detection (LOD) was in a range of 1 ng g_{TOC}^{-1}, and the limit of quantification (LOQ) in the range of 5 ng g_{TOC}^{-1}, both calculated based on S/N ratios in real sample matrix. Concentrations reported have been normalised to total organic carbon (TOC) to facilitate direct comparability across different sampling locations[31].

PTEs quantification. Solutions of the extracted PTEs were analysed via inductively coupled plasma mass spectrometry (ICP-MS; Thermo Scientific iCAP-Q) operated in helium collision cell mode with kinetic energy discrimination (KED). Element quantification was performed using a four-point external calibration curve. A total number of 7 elements were investigated (As, Ag, Cd, Te, Cr, Zn, and Pb) and their final concentrations reported as either milligrams or micrograms of the extracted element per kilogram of dry sample (mg kg^{-1} and µg kg^{-1}, respectively). Measurement uncertainties were determined from three replicate extractions and are expressed as standard deviations. Limits of detection (LOD) were obtained after the analysis of five procedural blank

samples (i.e., 2.5% HNO_3 solution processed through the full extraction protocol without sediment), defined as three times the standard deviation of the blank measurements[66].

Reagents, QA/QC procedures and data processing

All procedures related to sample and solution preparation were conducted under a laminar flow hood (Aura HZ72T, BIOAIR, Italy) to prevent airborne contamination. Sediments aliquots designated for organic analysis were handled using pre-cleaned glass of metal tools to minimise organic contamination; while inorganic elements were extracted from samples handled with low-density polyethylene (LDPE, Nalgene) bottles and testing tubes, meticulously cleaned and decontaminated. The cleaning process includes extended washing periods (48 h each) with a detergent solution (4 mL L^{-1} Nalgene L900) followed by rinsing with a 2% wt. HNO_3 and 0.01 M HCl solutions. The bottles were then rinsed three times with ultrapure water (Milli-Q from Sartorius Arium® mini, Germany; resistivity: 18.8 MΩ cm) and left to air-dry under a laminar flow hood. All organic solvents used for compounds extraction were purchased from Merck (Germany) and cleaned up by rectification over a 0.5 m packed column (reflux ratio approx. 1:25). Solvent purity was tasted by gas chromatographic analyses (purity over 99.9%). Ultrapure inorganic acids used in inorganic elements extractions were obtained from sub-boiling distiling using a Milestone (Shelton, USA) DuoPUR system[67]. Regarding organic compounds analysis, certified reference material for the identified compounds was purchased from Sigma-Aldrich (Germany) and peak correlations have been done with the graphical help of the software AMDIS32 (Automated Mass Spectral Deconvolution and Identification System), XCalibur™ (Thermo Fisher Scientific Inc., USA), and by hand. The limit of detection (LOD) was determined by S/N ratio >3. Data quality assurance (QA) and quality control (QC) protocols included laboratory blanks, triplicate samples and multiple runs per sample for geochemistry, TOC and PTEs extractions and quantifications. Furthermore, as detailed explained in the previous method paragraphs, internal standards and recovery percentages were employed for analytical control.

Calculations were carried out using Microsoft Excel spreadsheets. Statistical multivariate analysis concerning Principal Component Analysis (PCA) were performed using the Origin 2018 software (OriginLab Corporation, Northampton, MA, USA). Prior to PCA calculations, data normalisation was performed using z-score normalisation[68], represented by the Eq. (1):

$$z = (x - m)/\sigma, \quad (1)$$

where m is the average value of the variable data population, σ is the population standard deviation and x is the single value taken into consideration for the z-normalisation.

Normalisation was adopted to facilitate the identification of variations in variables across different samples, forcing a normal distribution of the dataset and the highlighting of potential geochemical anomalies. To uphold the reliability of the PCA results, principal components (PCs) with eigenvalues greater than 1 were retained, ensuring that only components representing substantial variance in the dataset were considered. This approach captured the majority of the dataset's variability, in line with established criteria for meaningful dimensionality reduction[69]. This systematic statistical approach facilitated the robust identification of correlations among distinct contaminant classes and key environmental parameters, including TOC, bathymetric depth, sediment flow accumulation, and basin morphology, thereby providing critical insights into the dominant processes regulating pollutant dynamics in this hadal ecosystem.

Received: 20 December 2025; Accepted: 4 March 2026;
Published online: 15 April 2026

References

1. Kioka, A. & Strasser, M. Oceanic trenches. in *Treatise on Geomorphology* 2nd edn (ed. Shroder, J. F.) 882–900. https://doi.org/10.1016/B978-0-12-818234-5.00167-X (Academic Press, 2022).
2. Du, M. et al. Geology, environment, and life in the deepest part of the world's oceans. *Innovation* **2**, 100109 (2021).
3. Jamieson, A. J., Fujii, T., Mayor, D. J., Solan, M. & Priede, I. G. Hadal trenches: the ecology of the deepest places on Earth. *Trends Ecol. Evol.* **25**, 190–197 (2010).
4. Xu, Y., Ge, H. & Fang, J. Biogeochemistry of hadal trenches: Recent developments and future perspectives. *Deep Sea Res. Part II Top. Stud. Oceanogr.* **155**, 19–26 (2018).
5. Chu, M. et al. Removal of dissolved organic carbon in the West Pacific hadal zones. *Nat. Commun.* **16**, 733 (2025).
6. Jamieson, A. *The Hadal Zone: life in the deepest oceans*. (Cambridge University Press, 2015).
7. Oguri, K. et al. Sediment accumulation and carbon burial in four hadal trench systems. *J. Geophys. Res. Biogeosci.* **127**, e2022JG006814 (2022).
8. Chu, M. et al. Earthquake-enhanced dissolved carbon cycles in ultra-deep ocean sediments. *Nat. Commun.* **14**, 5427 (2023).
9. Kioka, A. et al. Event stratigraphy in a hadal oceanic trench: the Japan trench as sedimentary archive recording recurrent giant subduction zone earthquakes and their role in organic carbon export to the deep sea. *Front. Earth Sci.* **7**, 319 (2019).
10. Zhang, X. et al. The hadal zone is an important and heterogeneous sink of black carbon in the ocean. *Commun. Earth Environ.* **3**, 1–9 (2022).
11. Liu, M. et al. Substantial accumulation of mercury in the deepest parts of the ocean and implications for the environmental mercury cycle. *Proc. Natl. Acad. Sci. USA* **118**, e2102629118 (2021).
12. Dasgupta, S. et al. Toxic anthropogenic pollutants reach the deepest ocean on Earth. *Geochem. Perspect. Lett.* **7**, 22–26 (2018).
13. Bacosa, H. P. et al. Marine snow aggregates are enriched in polycyclic aromatic hydrocarbons (PAHs) in oil contaminated waters: insights from a mesocosm study. *J. Mar. Sci. Eng.* **8**, 781 (2020).
14. Pohl, F., Eggenhuisen, J. T., Kane, I. A. & Clare, M. A. Transport and burial of microplastics in deep-marine sediments by turbidity currents. *Environ. Sci. Technol.* **54**, 4180–4189 (2020).
15. Gwiazda, R., Paull, C. K., Ussler, W. & Alexander, C. R. Evidence of modern fine-grained sediment accumulation in the Monterey Fan from measurements of the pesticide DDT and its metabolites. *Mar. Geol.* **363**, 125–133 (2015).
16. Chen, C. et al. Ocean as source or sink for legacy persistent organic pollutants. *J. Haz. Mat.* **486**, 136987 (2025).
17. Porz, L., Zhang, W. & Schrum, C. Natural and anthropogenic influences on the development of mud depocenters in the southwestern Baltic Sea. *Oceanolog* **65**, 182–193 (2023).
18. Bellanova, P., Schwarzbauer, J. & Reicherter, K. Inventory of aqueous and sediment-associated organic pollutants released by the 2021 flood in the Vicht–Inde catchment, Germany. *Environ. Sci. Eur.* **36**, 110 (2024).
19. Schwestermann, T. et al. Multivariate statistical and multiproxy constraints on earthquake-triggered sediment remobilization processes in the central Japan Trench. *Geochem. Geophys. Geosyst.* **21**, e2019GC008861 (2020).
20. Usami, K., *et al* The link between upper-slope submarine landslides and mass transport deposits in the hadal trenchs. Understanding and Reducing Landslide Disaster Risk: Volume 1 Sendai Landslide Partnerships and Kyoto Landslide Commitment 5th, 361-367 (2021)
21. Schwestermann, T. et al. Event-dominated transport, provenance, and burial of organic carbon in the Japan Trench. *Earth Planet. Sci. Lett.* **563**, 116870 (2021).

22. Kao, S. J. et al. Cyclone-driven deep sea injection of freshwater and heat by hyperpycnal flow in the subtropics. *Geophys. Res. Lett*. **37**, (2010).
23. Stow, D. A. V., Ogawa, Y., Lee, I. T. & Mitsuzawa, K. Neogene contourites, Miura-Boso forearc basin, SE Japan. in Deep-Water Contourite Systems: Modern Drifts and Ancient Series, Seismic and Sedimentary Characteristics (eds Stow, D. A. V., Pudsey, C. J., Howe, J. A., Faugères, J.-C. & Viana, A. R.) **22** (Geological Society of London, 2002).
24. Shah, S. B. Heavy metals in the marine environment - An Overview. in *Heavy Metals in Scleractinian Corals* (ed. Shah, S. B.) 1–26. https://doi.org/10.1007/978-3-030-73613-2_1 (Springer International Publishing, Cham, 2021).
25. Cui, J. et al. Occurrence of halogenated organic pollutants in hadal trenches of the Western Pacific Ocean. *Environ. Sci. Technol.* **54**, 15821–15828 (2020).
26. Shimanaga, M. & Yanagi, K. The Ryukyu Trench may function as a "depocenter" for anthropogenic marine litter. *J. Oceanogr.* **72**, 895–903 (2016).
27. Nakajima, R., Ikuta, T., Oguri, K. & Ritchie, H. Occurrence of polybrominated diphenyl ethers and benzotriazole UV stabilizers in the hadal amphipod *Hirondellea gigas*. *iScience* **26**, 107054 (2023).
28. Glud, R. N. et al. Hadal trenches are dynamic hotspots for early diagenesis in the deep sea. *Commun. Earth Environ.* **2**, 1–8 (2021).
29. Strasser, M. et al. Japan Trench event stratigraphy: first results from IODP giant piston coring in a deep-sea trench to advance subduction zone paleoseismology. *Mar. Geol.* **477**, 107387 (2024).
30. Peters, K. E., Walters, C. C. & Moldowan, J. M. *The Biomarker Guide* (Cambridge University Press, 2005).
31. Bellanova, P. et al. Contemporary pollution of surface sediments from the Algarve shelf, Portugal. *Mar. Pollut. Bull.* **176**, 113410 (2022).
32. Gough, M. & Rowland, S. Characterization of unresolved complex mixtures of hydrocarbons in petroleum. *Nature* **344**, 648–650 (1990).
33. Stout, S. A. et al. Characterization of naturally-occurring and anthropogenic PAHs in urban sediments – Wycoff/Eagle Harbor superfund site. *Environ. Forensics* **2**, 287–300 (2001).
34. Abdel-Shafy, H. I. & Mansour, M. S. M. A review on polycyclic aromatic hydrocarbons: source, environmental impact, effect on human health and remediation. *Egypt. J. Pet.* **25**, 107–123 (2016).
35. Wolska, L., Mechlińska, A., Rogowska, J. & Namieśnik, J. Sources and fate of PAHs and PCBs in the marine environment. *Crit. Rev. Environ. Sci. Technol.* **42**, 1172–1189 (2012).
36. Frenken, M., Bellanova, P., Nishimura, Y., Reicherter, K. & Schwarzbauer, J. Distribution of the geochemical signature caused by the 2011 Tohoku-oki tsunami in Misawa harbor, northern Japan. *Nat. Haz.* **114**, 313–333 (2022).
37. Tkalin, A. V. Chlorinated hydrocarbons in coastal bottom sediments of the Japan Sea. *Environ. Pollut.* **91**, 183–185 (1996).
38. Turusov, V., Rakitsky, V. & Tomatis, L. Dichlorodiphenyltrichloroethane (DDT): ubiquity, persistence, and risks. *Environ. Health Perspect.* **110**, 125–128 (2002).
39. Ebsa, G. et al. Degradation of Dichlorodiphenyltrichloroethane (DDT) and its main metabolites (Diphenyldichloroethylene (DDE) and Dichlorodiphenyldichloroethane (DDD) using Trichoderma species. *Process Biochem.* **151**, 74–87 (2025).
40. Schmidt, J. T. et al. Disentangling the history of deep ocean disposal for DDT and other industrial waste off southern California. *Environ. Sci. Technol.* **58**, 4346–4356 (2024).
41. Morisawa, S., Kato, A., Yoneda, M. & Shimada, Y. The dynamic performances of DDTs in the environment and japanese exposure to them: a historical perspective after the Ban. *Risk Anal.* **22**, 245–263 (2002).
42. Goto, A. et al. Multi-target analyses of persistent organic pollutants, halogenated natural products, and organophosphate esters in bivalves from Seto Inland Sea, Japan: residue levels, profiles, and spatial trends. *Sci. Total Environ.* **967**, 178801 (2025).
43. Wells, P. G. Biomonitoring the health of coastal marine ecosystems – the roles and challenges of microscale toxicity tests. *Mar. Pollut. Bull.* **39**, 39–47 (1999).
44. Zhang, M., Sun, X., Hu, Y., Chen, G. & Xu, J. The influence of anthropogenic activities on heavy metal pollution of estuary sediment from the coastal East China Sea in the past nearly 50 years. *Mar. Pollut. Bull.* **181**, 113872 (2022).
45. Miranda, L. S., Ayoko, G. A., Egodawatta, P. & Goonetilleke, A. Adsorption-desorption behavior of heavy metals in aquatic environments: influence of sediment, water and metal ionic properties. *J. Hazard. Mater.* **421**, 126743 (2022).
46. Lee, T. R., Wood, W. T. & Phrampus, B. J. A Machine Learning (kNN) approach to predicting global seafloor total organic carbon. *Glob. Biogeochem. Cycles* **33**, 37–46 (2019).
47. Hovikoski, J. et al. Bioturbation in the hadal zone. *Nat. Commun.* **16**, 1401 (2025).
48. Zheng, Y., Zhou, W., Xie, S. & Yu, X. A comparative study of *n*-alkane biomarker and pollen records: an example from southern China. *Chin. Sci. Bull.* **54**, 1065–1072 (2009).
49. Bellanova, P. et al. Anthropogenic pollutants and biomarkers for the identification of 2011 Tohoku-oki tsunami deposits (Japan). *Mar. Geol.* **422**, 106117 (2020).
50. McHugh, C. M. et al. Remobilization of surficial slope sediment triggered by the A.D. 2011 Mw 9 Tohoku-Oki earthquake and tsunami along the Japan Trench. *Geology* **44**, 391–394 (2016).
51. Oguri, K. et al. Hadal disturbance in the Japan Trench induced by the 2011 Tohoku–Oki Earthquake. *Sci. Rep.* **3**, 1915 (2013).
52. Kioka, A. et al. Megathrust earthquake drives drastic organic carbon supply to the hadal trench. *Sci. Rep.* **9**, 1553 (2019).
53. Molenaar, A., Moernaut, J., Wiemer, G., Dubois, N. & Strasser, M. Earthquake impact on active margins: tracing surficial remobilization and seismic strengthening in a slope sedimentary sequence. *Geophys. Res. Lett.* **46**, 6015–6023 (2019).
54. Ikehara, K., Usami, K. & Kanamatsu, T. Repeated occurrence of surface-sediment remobilization along the landward slope of the Japan Trench by great earthquakes. *Earth Planets Space* **72**, 114 (2020).
55. Ikehara, K., Irino, T. & Saito, Y. The 2011 Tohoku-oki tsunami-induced sediment remobilization on the Sendai shelf, Japan, from a comparison of pre- and post-tsunami surface sediments. *Sci. Rep.* **11**, 7864 (2021).
56. Miller, M. Breaking the slab. *Nat. Geosci.* **1**, 730–731 (2008).
57. Strasser, M. et al. Expedition 386 summary. *Proc. Int. Ocean Discov. Program* **386**, 1–62 (2023).
58. Arai, K., Inoue, T., Ikehara, K. & Sasaki, T. Episodic subsidence and active deformation of the forearc slope along the Japan Trench near the epicenter of the 2011 Tohoku Earthquake. *Earth Planet. Sci. Lett.* **408**, 9–15 (2014).
59. Kodaira, S. et al. Depth-varying structural characters in the rupture zone of the 2011 Tohoku-oki earthquake. *Geosphere* **13**, 1408–1424 (2017).
60. Kioka, A. & Strasser, M. Oceanic Trenches. in *Treatise on Geomorphology* 2nd edn (ed. Shroder, J. F.) 882–900 (Academic Press, 2022).
61. Strasser, M. et al. Expedition 386 methods. *Proc. Int. Ocean Discov. Program* **386**, 1–61 (2023).
62. Schwarzbauer, J., Littke, R. & Weigelt, V. Identification of specific organic contaminants for estimating the contribution of the Elbe river to the pollution of the German Bight. *Org. Geochem.* **31**, 1713–1731 (2000).
63. Deng, J., Feng, X. & Qiu, X. Extraction of heavy metal from sewage sludge using ultrasound-assisted nitric acid. *Chem. Eng. J.* **152**, 177–182 (2009).

64. Wang, Z., Fingas, M. & Li, K. Fractionation of a light crude oil and identification and quantitation of aliphatic, aromatic, and biomarker compounds by GC-FID and GC-MS, Part II. *J. Chromatogr. Sci.* **32**, 367–382 (1994).
65. Peters, K. E. & Moldowan, J. M. *The biomarker guide: interpreting molecular fossils in petroleum and ancient sediments* (Englewood Cliffs, 1993).
66. Binda, G. et al. Geochemical markers as a tool for the characterization of a multi-layer urban aquifer: the case study of Como (Northern Italy). *Water* **14**, 124 (2022).
67. Monticelli, D., Castelletti, A., Civati, D., Recchia, S. & Dossi, C. How to efficiently produce ultrapure acids. *Int. J. Anal. Chem.* **2019**, e5180610 (2019).
68. Binda, G. et al. Integration of photogrammetry from unmanned aerial vehicles, field measurements and discrete fracture network modeling to understand groundwater flow in remote settings: test and comparison with geochemical markers in an Alpine catchment. *Hydrogeol. J.* **29**, 1203–1218 (2021).
69. Maćkiewicz, A. & Ratajczak, W. Principal components analysis (PCA). *Comput. Geosci.* **19**, 303–342 (1993).
70. Uchida, N. & Bürgmann, R. A decade of lessons learned from the 2011 Tohoku-Oki Earthquake. *Rev. Geophys. Sci.* **59**, e2020RG000713 (2021).

Acknowledgements

The authors are thankful to the European Union - NextGenerationEU - Mission 4 “Education and Research” - Component 2 “From Research to Business” - Investment 3.1 “Fund for the realisation of an integrated system of research and innovation infrastructures” – Project IR0000037 - GeoSciences IR - CUP I53C22000800006, for providing a scholarship to the first author to undertake this study. Scientific support from CRIETT centre of University of Insubria (instrument code: MAC10) is greatly acknowledged. This study would not have been possible without the dedication and hard work of the crew and scientific party of IODP Expedition 386. The research was supported by DFG grant 565848016.

Funding

Open Access funding enabled and organized by Projekt DEAL.

Competing interests

The authors declare no competing interests.

Additional information

Supplementary information The online version contains supplementary material available at https://doi.org/10.1038/s43247-026-03401-6.

Correspondence and requests for materials should be addressed to Piero Bellanova.

Peer review information *Communications Earth and Environment* thanks Kiichiro Kawamura and Luis Somoza for their contribution to the peer review of this work. Primary Handling Editor: Nandita Basu. A peer review file is available.